



HAL
open science

SMOS salinity in the subtropical North Atlantic salinity maximum. Part II: Two-dimensional horizontal thermohaline variability

Nicolas N. Kolodziejczyk, Olga Hernandez, Jacqueline Boutin, Gilles Reverdin

► To cite this version:

Nicolas N. Kolodziejczyk, Olga Hernandez, Jacqueline Boutin, Gilles Reverdin. SMOS salinity in the subtropical North Atlantic salinity maximum. Part II: Two-dimensional horizontal thermohaline variability. *Journal of Geophysical Research. Oceans*, 2015, 120 (2), pp.972-987. 10.1002/2014JC010103 . hal-01121855

HAL Id: hal-01121855

<https://hal.sorbonne-universite.fr/hal-01121855v1>

Submitted on 2 Mar 2015

HAL is a multi-disciplinary open access archive for the deposit and dissemination of scientific research documents, whether they are published or not. The documents may come from teaching and research institutions in France or abroad, or from public or private research centers.

L'archive ouverte pluridisciplinaire **HAL**, est destinée au dépôt et à la diffusion de documents scientifiques de niveau recherche, publiés ou non, émanant des établissements d'enseignement et de recherche français ou étrangers, des laboratoires publics ou privés.

SMOS salinity in the subtropical North Atlantic salinity maximum.

Part II: Two-dimensional horizontal thermohaline variability

Nicolas Kolodziejczyk¹, Olga Hernandez¹, Jacqueline Boutin¹ and Gilles Reverdin¹

submitted in *Journal of Geophysical Research – Ocean*

¹Sorbonne Universités (UPMC, Univ Paris 06)–CNRS–IRD–MNHN, LOCEAN Laboratory, 4

This article has been accepted for publication and undergone full peer review but has not been through the copyediting, typesetting, pagination and proofreading process which may lead to differences between this version and the Version of Record. Please cite this article as doi: 10.1002/2014JC010103

© 2015 American Geophysical Union
Received: Apr 30, 2014; Revised: Dec 13, 2014; Accepted: Jan 14, 2015

place Jussieu, F-75005, Paris, France

Corresponding author: Dr. Nicolas Kolodziejczyk, E-mail: nicolas.kolodziejczyk@gmail.com

Accepted Article

Abstract:

The horizontal thermohaline seasonal variability of the surface ocean is investigated in the subtropical North Atlantic Surface Salinity Maximum (SSSmax) region. Satellite sea surface temperature and salinity are used, along with high-resolution thermosalinograph data, and Argo interpolated products, to study the horizontal two-dimensional field of density and thermohaline variability.

During late winter, compensated temperature and salinity gradients at large and mesoscale are observed northeast of the SSSmax, in the Azores Front Current region. In spite of the large and sharp surface thermohaline fronts, satellite measurements reveal a rather weak surface horizontal density gradient. During summer, the front is dominated by salinity gradients. South of the SSSmax, at large scales, the density ratio is controlled by the salinity gradient and the horizontal density gradient is enhanced by a constructive contribution of opposite salinity and temperature gradients.

1 Introduction

The global distribution of the mixed layer horizontal thermohaline contrasts, *i.e.* the temperature and salinity variations, have been shown to vary as a function of location, time and spatial scales. At large scales within subtropical latitudes, the temperature variability dominates the seasonal surface density changes through the seasonal cycle of solar heat flux (*Johnson et al.*, 2012). Thus, the buoyancy gradient is periodically driven at large scales by temperature variability (*Stommel*, 1993). In the tropics, high precipitation and river plumes produce strong yet shallow vertical and horizontal gradients in the upper ocean (e.g.: *Reverdin et al.*, 2007; *Tanguy et al.*, 2010; *Mignot et al.* 2012; *Grodsky et al.*, 2014a). In addition, surface horizontal density gradients are directly related to the dynamics of the mixed layer and upper ocean, due to the thermal wind relation. At mesoscales, the surface thermohaline structures are mainly driven by baroclinic instability of the currents located at frontal regions, with this instability the main source of the mesoscale meanders and eddies in the world ocean. Oceanic mesoscale eddies contribute to important horizontal heat and salt contrasts and transports on a global scale (*Dong et al.*, 2014). Mesoscale fronts also contribute to the cascade towards smaller scales, *i.e.* submesoscales, so that mixing ultimately diffuses the horizontal density field and reduces the horizontal density gradient (*Young*, 1994; *Rudnick and Martin*, 2002).

As a first order, the density fluctuations can be written as a linear combination of the temperature and salinity fluctuations :

$$\Delta\rho = \rho_0 \beta \Delta S - \rho_0 \alpha \Delta T \quad (1)$$

where α and β are the coefficients of thermal expansion and of haline contraction of sea water, and $\rho_0 = 1025 \text{ kg.m}^{-3}$ is the reference density (*e.g.*: Yeager and Large, 2007); the terms $\Delta\rho$; $\Delta\theta$ and ΔS are the respective horizontal differences of potential density, potential temperature and salinity of sea water. In this context, a measure of the relative effect of temperature and salinity on density is given by the density ratio:

$$R = \frac{\alpha \Delta\theta}{\beta \Delta S} \quad (2)$$

In the horizontal plane, a density ratio of $R=1$ indicates that the horizontal gradients of temperature and salinity have compensated effects on the density gradient. In this case, the thermohaline front could be sharp while the density gradient remains weak, thus playing a weak dynamical role. A density ratio $R > 1$, indicates that the temperature gradient has a dominant effect on the density gradient, while a density ratio of $R < 1$ corresponds to a dominant effect of the salinity gradient.

At large scales, between 20–50° N in the three oceanic basins, Stommel (1993) noted that during winter, the density ratio averages around $R=2$. However, for thermohaline fronts between 10 m and 100 km wavelength, historical and recent observations have established that, during winter, the surface thermohaline structures are often compensated in subtropical eastern oceanic regions (*e.g.*: Roden, 1974; 1991; Rudnick and Luyten, 1996; Rudnick and Ferrari,

1999; Ferrari and Rudnick, 2000; Rudnick and Martin, 2002).

In the North Atlantic Ocean, the poleward zonal boundary of the subtropical SSS_{max} waters appears to be the Azores Front/Current (Alves and Colin de Verdière, 1999; Julianno and Alves, 2007). The Azores Current is a permanent eastward flow centered around 34° N, reaching the Gulf of Cadiz with an annual mean surface velocity of about 6 cm s⁻¹. It meanders along its trajectory, revealing a tendency for the formation of cyclonic meanders on the northern side of its main axis and anticyclonic meanders on the southern side (Julianno and Alves, 2007). Indeed, in the region between of 21–25° W, Rudnick and Luyten (1996) have shown that the Azores front is a region where density compensated water masses with a large mesoscale thermohaline variability subduct, *i.e.* denser water masses and their thermohaline anomalies slide southward below the lighter water masses.

However, these previous observations are only located in small areas, typically along 1D individual ship transects. A recent global study of the 2D horizontal near surface Turner angle (basically the *atan* of the density ratio; Johnson *et al.*, 2012) computed from Argo temperature and salinity profiles suggests large spatial and temporal variability. Unfortunately, the Argo array provides insufficient sampling in some areas of primary interest (e.g. Amazon–Orinoco plumes, frontal regions), and its resolution (nominally 300–500 km) is too coarse to resolve the mesoscale water mass contrasts.

The recently launched (late 2009) Soil Moisture and Ocean Salinity (SMOS) satellite mission (Font *et al.*, 2010) provides microwave measurements of two-dimensional salinity fields of the surface ocean at a less than 100 km resolution, unmatched by existing in situ networks. Until now, much focus has been put at investigating mesoscale structures revealed by SMOS in areas of high thermohaline contrasts such as the Gulf Stream region (Reul *et al.*, 2014), the Amazon plume, the Panama upwelling (see a review in Reul *et al.*, 2013). Here, for the first time, we use SMOS SSS in combination with microwave SST from Tropical Microwave Imager (TMI) to investigate the mesoscale thermohaline variability at scales of hundred kilometers in the open ocean. Actually, with a monthly and at a 100x100km² resolution, *i.e.* achieving a better spatial resolution than Argo sampling, SMOS SSS have been shown to reach an accuracy of about 0.15–0.20 (in Practical Salinity Scale PSS-78) in the tropical and subtropical regions (Hasson *et al.* 2013; Hernandez *et al.*, 2014). Nevertheless, in coastal regions, SMOS data are strongly affected by anthropogenic radio frequency interferences (RFI) (Oliva *et al.*, 2012) which act to introduce bias into the resulting SSS data (Reul *et al.* 2012; Boutin *et al.*, 2013). There are also seasonal and latitudinal biases likely linked to the imperfect correction of geophysical signals (e.g. galactic noise) backscattered by the sea surface, and additionally, direct solar heating of the instrument's antenna (Kainulainen *et al.*, 2012).

The goal of this study is to characterize both the sea surface thermohaline structures and the seasonal variability of the subtropical Atlantic at spatial resolutions ranging from the mesoscale to basin-wide scales. In order to test the new mesoscale measurements provided by

the SMOS satellite products we focus on the northern SSSmax along the Azores Front/Current which is an open-ocean region featuring frequent mesoscale thermohaline front and eddies.

The paper is organized as follows. Data and Methodology are presented in Section 2. The large scale thermohaline variability as observed from Argo interpolated products and satellite products are presented and discussed in section 3. The mesoscale variability of surface thermohaline structures over the north of SSSmax and in the region of the Azores Front/Current is validated and presented in section 4. Results are discussed and summarized in section 5.

2 Data and methodology

2.1 Data

2.1.1 Thermosalinograph T/S data

High resolution near-surface (5 m depth of intake) temperature and salinity data within the subtropical north Atlantic SSSmax region are provided by thermosalinographs (TSG) mounted on the merchant vessels *Toucan* and *Colibri*. Since 1994, temperature and salinity data were collected along northeast to southwest transects across the North Atlantic subtropical SSSmax from western Europa to northern South America (Fig. 1). The nominal horizontal resolution is around 2.5 km, and the journey between Europa and South America typically lasts 10 days. The data are systematically post-calibrated with collocated CTD, Argo data and water samples, when

they are available, and provided with flags by the french Service d'Observation of SSS (<http://www.legos.obs-mip.fr/observations/sss>), thus, the error is on the order of 0.02–0.08. Only data with "Adjusted" and "Good" or "Probably Good" flags data are used in this study, and transects with too much flagged bad data have been systematically removed (Table 1). When it is possible, the missing values are replaced by linearly interpolated values. Therefore, from 2010 to 2011, only 14 transects are used (Table 1).

2.1.2 ISAS product

Monthly gridded fields of temperature and salinity are derived from the ISAS (In Situ Analysis System) dataset, an optimal estimation tool designed for the synthesis of the Argo global dataset (*Gaillard et al.* 2009). The version used in this study is the V6-D7CA2S0 (*Gaillard*, 2012, documentation available at <http://wwz.ifremer.fr/lpo/La-recherche/Projets-en-cours/GLOSCAL/Global-T-S-analysis>), which covers the 2004–2012 period and, thus overlapping with SMOS measurements between 2010–2012. The gridded fields were produced over the global ocean 70° N–70° S on a 1/2° grid by the ISAS project with datasets downloaded from the Coriolis data center (for more details on ISAS see *Gaillard et al.*, 2009). The major contribution to the data set is from Argo array of profiling floats, reaching an approximate resolution of one profile every 10–days and every 3–degrees over the SMOS period (www.argo.ucsd.edu). The optimal interpolation is computed over a 1/2° grid, but involves a structure function modeled as the sum of two Gaussian functions, each associated with specific

time and space scales, resulting in a smoothing over typically 3 degrees. The smallest scale which can be retrieved with ISAS analysis is thus not smaller than 300 km. The surface temperature and salinity fields used in our study are mostly extrapolated from the shallowest Argo measurements at about 5 m depth.

2.1.3 Satellite data

2.1.3.1 SMOS SSS data

In the present study, SMOS SSS are the 'CATDS-CEC LOCEAN 2013' monthly gridded product for the period June 2010 to December 2012 (data freely available on request on support@catds.fr). The SMOS technical characteristics, measurements and validation are described in the companion paper by *Hernandez et al.* (2014). The gridded maps are obtained with a running-average 2D window over $100 \times 100 \text{ km}^2$ and oversampled every $1/4^\circ$, thus allowing high resolution observations of the synoptic variability of SSS to be made (*Boutin et al.*, 2013). This is a marked improvement over interpolated Argo data products, which feature a $\sim 300\text{--}500$ km resolution. After correcting the monthly bias in the Salinity Process in the Upper Ocean Region Study (SPURS) region (<http://spurs.jpl.nasa.gov/SPURS/index.jsp>), the calculated RMSE of the monthly $100 \times 100 \text{ km}^2$ SMOS SSS collocated with *in situ* TSG SSS down-sampled to the SMOS spatial resolution was estimated to be around 0.15 (*Hernandez et al.*, 2014). The impact of this SSS error on the density and horizontal density gradient is on the order of 0.1 kg.m^{-3} and $10^{-6} \text{ kg.m}^{-4}$, respectively.

The SMOS monthly SSS performs well in the region of the Azores Front/Current between 25–45° W (Fig. 1; *Hernandez et al.*, 2014) characterized by relatively strong thermohaline gradients associated with mesoscale frontal eddies and meanders of hundred kilometers scales with propagation velocities of about 2.5 cm.s⁻¹ (*Alves and Colin de Verdière*, 1999). This region thus appears to be a convenient benchmark for validating SMOS mesoscale SSS. Furthermore, the Azores Front/Current is located far from the coast in the center of the subtropical basin, a region where SMOS SSS data are only weakly affected by RFI and coast contamination (*Hernandez et al.*, 2014).

The SMOS/TMI and ISAS thermohaline fields are first compared with TSG temperature and salinity transects within two ranges of length scales: larger than 500 km and between 200–500 km, respectively. 1D spectral 500 km lowpass (LPF) and 200–500 km bandpass (BPF) 2nd order Butterworth filters are used. The shorter wavelength of 200 km corresponds to the Nyquist wavelength value for the 100x100km² monthly SMOS salinity fields.

To reduce the noise in computing maps of thermohaline gradients, a 2D windows average filter are used. In section 3 (section 4), the SMOS/TMI maps are filtered with 2D 3° x3° (2° x2°) average windows. At large scales, the 3° x3° smoothing of SMOS and TMI data basically fits the nominal target resolution of the Argo array (~300 km, *Gaillard et al.*, 2009). At mesoscales (Section 4.2), although the monthly unfiltered temperature, salinity and density maps

are shown, the density gradients and density ratio are computed from $2^\circ \times 2^\circ$ window averaged fields, in order to reduce the noise in gradients computation.

2.1.3.2 TMI SST data

The TMI SST are derived from remote measurements of a microwave radiometer on board the Tropical Rainfall Measuring Mission (TRMM) satellite (documentation and data freely available on www.remss.com). The important feature of microwave retrievals is that SST can be measured through clouds, owing to their near transparency at wavelengths of 10.7 GHz. TMI SST data used in this study are weekly and monthly mean maps products between June 2010 and December 2012, during the SMOS period. TMI data resolve the SST at $1/4^\circ \times 1/4^\circ$ between 40° N-S within the Tropical belt. The TMI SST have a 0.08° C bias and 0.57° C standard deviation when compared to TAO and PIRATA buoys *in situ* measurements (*Gentemann et al.*, 2004).

2.1.3.3 AVISO surface currents

The monthly map of surface geostrophic velocities in the Azores Front/Current region, were derived from the multi-mission AVISO $1/3^\circ \times 1/3^\circ$ gridded weekly delayed time surface geostrophic current mapped products (the products named `dt_upd_global_merged_msla_uv_*`

downloaded from www.aviso.altimetry.fr). RMS differences between AVISO and available *in situ* drifting buoy measurements is less than 13 cm.s^{-1} (Rio *et al.*, 2011). This accuracy is sufficient in the present study, since we consider surface velocities of cyclonic and anticyclonic features on the order of 20 cm.s^{-1} .

2.1.3.4 MODIS Chlorophyll-a data

Monthly MODIS/Aqua Level 3 Chlorophyll-a data were downloaded from the NASA OceanColor Home Page (<http://oceancolor.gsfc.nasa.gov/>). The operational algorithm for deriving near-surface chlorophyll-a concentrations (OC; O'Reilly *et al.* 2000) was updated using *in situ* data from NOMAD version 2. NOMAD is a publicly available, global bio-optical data set constructed from data archived in SeaBASS. The algorithm form describes the polynomial best fit that relates the log-transformed geophysical variable to a log-transformed ratio of remote-sensing reflectance. The Level 3 Standard Mapped Image (SMI) products are image representations of binned data products. This image is typically a scaled value (16bit), two-dimensional array on an Equidistant Cylindrical projection of the globe.

2.2 2-D density ratio

In order to compute the horizontal surface density ratio without taking any arbitrary

direction for the horizontal gradient, we have chosen to define the complex ratio for each month, following *Ferrari and Paparella* (2003)

$$R = \frac{\alpha(\theta_x + i.\theta_y)}{\beta(S_x + i.S_y)} \quad (3)$$

where α is the thermal expansion; β the haline contraction coefficients of sea water, θ the temperature, S the salinity, and x and y indicate the derivative along zonal and meridional axes, respectively. The phase Φ of the complex density ratio R quantifies the degree of alignment of θ and S gradients. If the phase is $\Phi=0^\circ$ or $\Phi=180^\circ$, then there is thermohaline alignment. The magnitude of R quantifies the relative strength of the gradients of θ and S . If $|R| = 1$ and $\Phi=0^\circ$, then temperature and salinity cancel each other in the buoyancy balance and there is thermohaline compensation. A density ratio $|R|>1$, indicates that the temperature gradient has a dominant effect on the density gradient, while a density ratio of $|R|<1$ corresponds to a dominant effect of the salinity gradient (see Table 2).

In the present study, the median of $|R|$ is preferred because it is less sensitive to outliers of $|R|$ than the mean calculation (*Ferrari and Rudnick*, 2000). The mean angle/phase of complex R , Φ , are computed, taking the mean of the circular quantities Φ_i defined as (*Fisher*, 1993):

$$M_\phi = \text{atan2} \left\{ \frac{1}{N} \sum_T \sin \Phi_i, \frac{1}{N} \sum_T \cos \Phi_i \right\} \quad (4)$$

where atan2 is the four-quadrant inverse tangent, Φ_i is an element of the angles sample; N is the size of the angles sample.

3 Large scale thermohaline structures

During August 2011, the comparison of the 500 km LPF temperature, salinity and density among TSG, SMOS, TMI and ISAS surface salinity, show a reasonable agreement (Fig. 2a-c). The large scale normalized horizontal gradients (Eq. 1), are also well observed using SMOS and TMI satellite data (Fig. 2d-f). In spite of unexpected peaks in SMOS-derived gradient north of 35° N, it captures the variations of the gradient south of 35° N, which are not well reproduced from ISAS (Fig. 2d). Satellite measurements thus allows a more accurate computation of the density gradient (Fig. 2e) and of the density ratio (Fig. 2f).

A more systematic correlation computation of the horizontal gradients between SMOS/TMI, ISAS and the available TSG transects over the 14 transects over the period 2010-2011 (0.90 ± 0.08 and 0.91 ± 0.05 , respectively; Fig. 3a, b and Table 3) reveals that, on average, both ISAS and SMOS perform well in the 500 km low pass filtered spatial salinity structures with significant correlation coefficients at the 99% level for each individual correlation in the Table 3. However, along the ship transects the horizontal temperature gradients derived from TMI exhibit a better correlation (0.83 ± 0.12) than for the ISAS ones (0.70 ± 0.19), likely explained by the better sampling of satellite measurements over Argo array in some regions (Fig. 3c,d and Table 3).

ISAS and the $3^{\circ} \times 3^{\circ}$ smoothed satellite maps fields provide a 2D overview of the near

surface salinity, temperature and density in the northern subtropical Atlantic during boreal winter (March 2011–2012) and summer (August 2010–2011–2012) (Fig. 4). The position of the SSSmax is defined within isohaline contours 37.0 (thick black contours; Fig. 4).

In March, although SMOS SSS is slightly saltier than ISAS salinity (around 0.1; Fig. 4a,b), the horizontal structure of salinity distribution is qualitatively in agreement with the SSSmax centered around 35° W–24° N. In the western tropical Atlantic, close to the Amazon–Orinoco mouth, SMOS data reveal fresher surface water, which results in a sharper salinity front than reported with ISAS products. Near the eastern boundary, SMOS salinities appear to be fresher than ISAS. This is however possibly due to continent vicinity which introduces negative biases up to about 800 km from the coast and possibly to unfiltered RFIs. The large scale northeast/southwestward gradient of SST is visible from both TMI and ISAS fields (Fig. 4c, d), and explain the horizontal distribution of surface density observed (Fig. 4e,f).

During March, the strongest surface density gradient is observed at the equatorward rim of the SSSmax, south of 24° N. (Fig. 5). This is mainly explained by a small $|R| < 1$ occurring within a band between 15–24° N (Fig. 5c, d) whilst the surface horizontal temperature and salinity gradients are in opposite sense (Fig. 5e,f). In contrast, north of 24° N, temperature and salinity gradients are aligned and in the same direction ($M_{\phi} \sim 0^{\circ}$; Fig. 5e,f) and the temperature contribution to the density gradient is largest ($|R| > 1$; Fig. 5c,d). More specifically, within the north-eastern part of the SSSmax (north of 24° N and east of 40° N), the lowest values of surface density gradient are observed ($2 \cdot 10^{-7} \text{ kg.m}^{-4}$). This can be explained by strongly

compensated horizontal surface properties found in both satellite and ISAS maps during wintertime ($R \sim 1$; Fig. 5c). Along 34° N, density gradients larger than $0.6 \cdot 10^{-6} \text{ kg.m}^{-4}$ are observed in both ISAS and SMOS (Fig. 5a, b). This density frontal region is related to the subtropical Azores Front (*Juliano and Alves, 2007*).

In contrast, during summer, the SSS maximum is slightly shifted northward, while in the tropics the SSS decreases because of high precipitations in the ITCZ around 8° N and also because the intensification of the Amazon–Orinoco freshwater discharge (Fig. 4g,h; *Reverdin et al., 2007*). SMOS SSS exhibits also lower values and sharper salinity fronts than ISAS SSS over the freshwater plume of the Amazon–Orinoco (more than 1.0 salinity unit). During August, the main seasonal contrast is observed in the temperature fields, with warmer SSTs observed over the entire subtropics, (more than 5° C higher than comparable winter SSTs Fig. 4i, j). This observation explains the summer distribution of surface density (Fig. 4k, l) being more closely related to the SSS distribution than SST, and showing a large decrease of surface density with no values greater than $\sigma_\theta = 25.5 \text{ kg.m}^{-3}$ (Fig. 4k,l). Indeed, north of 24° N, the summer atmospheric heating reduces the north–south temperature gradient ($R < 1$, Fig. 5g,l) and the density gradient is now dominated by variations in salinity (Fig. 5h, l). In the south–western tropics, strong enhancing of the density front due to increase of freshwater intrusion from Amazon–Orinoco river during the summer season, can also be observed ($R \ll 1$; Fig. 5g,h,i,j).

4 Mesoscale thermohaline variability

4.1 Validation of mesoscale variability

During August 2011, in the range of 200–500 km scales, the horizontal gradients of temperature, salinity and density reveal a very good agreement between SMOS/TMI and TSG data (Fig. 6a,b, c), whilst mesoscales features are unresolved within the ISAS data (Fig. 6a, b). However, discrepancies are locally visible around 20° N and north of 35° N, which are likely attributable to noise in both SMOS SSS and TMI SST data. This mismatch could also be due to lack of synopticity of the monthly averaged satellite products, contrasting the TSG data, which provide a 'snapshot' sampling as the ships travel approximately 500 km per day. At these scales, surprisingly, the thermohaline variability retrieved with satellite data are not significantly better correlated with TSG features (0.47 ± 0.24 for SMOS and 0.53 ± 0.33 for TMI SST at 99% for each individual correlation; Fig. 7 and Table 4) than with ISAS (0.20 ± 0.29 and 0.18 ± 0.32 for salinity and temperature, respectively; Table 4).

4.2 Example of 2D thermohaline mesoscale structures : the Azores Front/Currents

In order to further validate and illustrate the capability of SMOS and TMI at sampling 2D mesoscale features, we focus on the region of the Azores Front/Current between 25–40° N/25–45° W. Other dynamical (AVISO currents and vorticity) and tracer fields (Chlorophyll-a) have also been used to identify and compare observed mesoscale features observed within this area.

In this region, the meridional position of the core of the Azores Front/Current is identified using the AVISO surface currents and vorticity values of $8 \cdot 10^{-5} \text{ s}^{-1}$ (thick black line; Fig. 8a,c). During late winter, in March 2012, the Azores front can be identified by the isohaline 36.6 and the 19° C isotherm using the monthly SMOS SSS and TMI SST (Fig. 8a,c), at much higher resolution than possible using ISAS T and S fields (Fig. 8b and d) .

The satellite derived surface density reveals interesting contrasted features: i) west of 38° W , the Azores front is well marked in density (Fig. 8a, b), ii) while it is more diffuse east of 38° W . This is explained by the temperature gradient which dominates the horizontal density gradient ($R > 2$; Fig. 9ab). East of 38° W , the density front is less defined because horizontal salinity and temperature gradients are well aligned ($\phi_R \sim 0^\circ$; Fig. 9c) and more compensated ($R \sim [0.7, 1.5]$; Fig. 9b). This explains the similarity between the temperature and salinity front and mesoscale features found east of 38° W during March 2012 (Fig. 8a,b). The presence of this mesoscale feature is independently confirmed within the ISAS fields, albeit smoothed by the interpolation method and the sparse distribution of Argo data (Fig. 8b, d).

During July 2011, the surface thermohaline signature of the Azores front is only observable from SSS (Fig. 10), due to large scale summer heating over the whole subtropics. This results in the surface horizontal SST gradients turning east–west, by about 90° , versus the winter season (Fig. 8). In order to further validate the mesoscale features, the high resolution

monthly Chlorophyll-a MODIS data have been considered (Fig. 10e). The meandering front and associated eddies observed in current, Chl-a and salinity fields are generally consistent. This can be observed west of 30° W, where a series of high (low) salinity and low (high) chlorophyll-a signed anticyclonic (cyclonic) eddies are observed (Fig. 10a,c,d,e).

East of $35-30^{\circ}$ W, the intensified surface density gradient appears to be mainly controlled by the surface heating (Fig. 10f,g, and Fig. 11a). Both northward and southward of the Azores this intensification of the gradient is mainly explained by the out of phase SST and SSS gradients ($\phi_R \sim 145-145^{\circ}$; Fig. 11c): both contributing to enhance the surface density gradient and exhibiting a comparable amplitude ($R \sim 1$; Fig. 11b). Along the Azores front, the SSS gradient contribution is larger than the SST gradient one ($R < 1$; Fig. 11b), while the SST and SSS gradient are no more well aligned ($\phi_R \sim -20-90^{\circ}$; Fig. 11c).

5 Discussion and conclusion

The analysis of monthly surface horizontal thermohaline structures in the tropical-subtropical SSSmax from SMOS SSS and TMI SST reveal a significantly improved spatial and temporal resolution than previously possible using interpolated Argo based products (*Johnson et al.*, 2012). The availability of SMOS has thus, for the first time, enabled the possibility of observing the 2D surface mesoscale thermohaline variability of the oceanic fronts from space, as

illustrated in the Azores Front/Current region.

In order to measure the capability of SMOS SSS and TMI SST products at monitoring large-scale and mesoscale variability, the surface horizontal thermohaline variability has been compared with the one derived from TSG and ISAS products. At large scale, ISAS and SMOS/TMI products are broadly comparable, but SMOS and TMI offer substantial advantages when resolving surface mesoscale features over Argo based products. For example, in the region of the Amazon–Orinoco plume the correlation between SMOS and TSG salinity are often better than from ISAS salinity.

However, an important caveat is that SMOS and TMI microwave radiometers measure SSS and SST within respectively the first centimeter and millimeters of the sea surface. As a consequence, stratification and boundary layers can lead to unresolved differences when completing inter-comparisons between these products and deeper data (typically 5 m) from Argo or TSG. In particular, large differences may be observed in regions of very shallow mixed layer and strong near surface vertical temperature and salinity gradient, such as the freshwater river plumes and high precipitation region (*Mignot et al., 2012*). For mesoscale features evolving at time scales lower than 1 month, the lack of synopticity of the monthly products from ISAS and satellite data could be responsible for the differences from the TSG observations which are quasi-instantaneous at mesoscale.

At large scales, two regions can be separated in the SSSmax region. Northward of the SSSmax (north of 25° N), the thermohaline structures reveal a clear alignment and opposite effects of surface horizontal temperature and salinity gradients, which exhibits compensation in the northeast during boreal winter (*Johnson et al.*, 2012). South of the SSSmax (south of 25° N), the temperature and salinity gradients constructively enhance the horizontal density gradient that is mainly controlled by the salinity gradient. In these regions the meridional gradient of E-P atmospheric flux and intensive Amazon–Orinoco run-off advection imply large scale forcing (*Reverdin et al.*, 2007; *Grodsky et al.*, 2014a; *Grodsky et al.*, 2014b) that generates opposite gradients of temperature and salinity.

At mesoscales, we focused on the Azores Front/Current region in order to show the SMOS capability in a region featuring strong mesoscale signatures in SSS, SST (during winter), vorticity and Chlorophyll-a (during summer). First, the different products of dynamical and passive tracers in such frontal region correspond well with SMOS-observed SSS mesoscale structures. Second, the Azores front retains its signature in salinity all along the year, whereas SST or Chlorophyll-a do not (not shown). Third, during the winter (March), at large to mesoscale the thermohaline gradients are well aligned and compensated in this region, except north of the front over a thin band along 36° N.

The present study shows that the winter horizontal thermohaline gradient is compensated through the range of 200 to 500 km wavelengths, while *Rudnick and Ferrari* (1999) established

the thermohaline compensation in the mixed layer of the subtropical North Pacific at wavelengths as short as 10 m and up to 10 km. During winter in the eastern Azores front region, *Rudnick and Luyten* (1996) suggest also that thermohaline compensation is likely to occur at all scales larger than 10 km. Furthermore, the compensation is also very sensitive to the seasonal variability: it is established during late winter (March) and rapidly disappears during April (not shown). This variability can be further investigated with the available SMOS SSS data set. Additional work investigating the thermohaline variability at scales between 10 and 100 km from TSG data will be required to fill the gap between our study and *Rudnick and Ferrari* (1999) and document temporal evolution of the mesoscale to submesoscale thermohaline surface variability. This is left for a further study.

Contrary to the investigation of *Rudnick and Luyten* (1996) east of 25° W, west of 25° W, we found that the winter alignment and compensation occur mainly on and south of the Azores front, while they found the largest spiciness (density compensated water masses) signal north of the front within the subducting denser water masses in January and February. Furthermore, they suggest that such a spiciness signal could be due to the straining of the tracers along isopycnal. Other processes could be at work in explaining the horizontal compensation at and south of the front. During winter, the observed horizontal alignment and compensation at and south of the front may be primary due to the surface cooling over the subtropical north SSSmax and the mean southward meridional gradient of surface salinity. At smaller-scale, it could also be achieved through strong vertical and horizontal mixing (Busecke

et al, 2014), ubiquitous in the eastern subtropical regions under winter cooling, and destabilizing salinity vertical gradient (Marshall and Schott, 1999; Ferrari and Paparella, 2003; Cole et al., 2010; Yeager and Large, 2007; Kolodziejczyk and Gaillard, 2013).

The advection of thermohaline surface mesoscale features could also have an impact on the subducted water masses (Rudnick and Luyten, 1996; Busecke et al., 2014; Gordon and Giulivi, 2014). At subtropical latitudes, some authors have shown that the relation between temperature and salinity, the density ratio, is conserved between the surface and the interior, suggesting that the ocean interior waters are probably linked with the sea surface ones during winter (Iselin, 1939). During late winter, the mixed layer is deepest and densest, so that it communicates most efficiently with the ocean interior (Stommel, 1979). It has been shown that the strongly compensated thermohaline structures can be transmitted from the deepest mixed layer to the layer below (Rudnick and Luyten, 1996; Cole et al., 2010; Cole and Rudnick, 2012; Bingham et al., 2012). Highly density-compensated waters can also be formed directly at the base of the mixed layer through vertical convective mixing (Yeager and Large, 2007; Kolodziejczyk and Gaillard, 2013). In each case, the subducted/injected interior anomalies of temperature, salinity, and density are related to mixed layer late winter thermohaline properties contrasts and associated mechanisms.

Although this study shows encouraging results on resolving mesoscale with SMOS monthly fields, observation at shorter time scale is needed to resolve the thermohaline

mesoscale features more accurately at lower latitude (*Chelton et al.*, 1998). Figure 12 shows the 10 day SMOS SSS and weekly TMI SST fields between the 11–21 March 2011, and the density as deduced from satellite measurements (Fig. 12e,f). The left panel presents a zoom in the region of the Azores front which exhibits a ubiquitous mesoscale filament of temperature and salinity observed over a 10–day period (Fig. 12b, d). However, this feature is not well observable with the density computed from satellite measurements (Fig. 12f). This suggests the compensating contribution of temperature and salinity fronts.

In conclusion, the present study shows that the joint satellite remote microwave radiometer measurements of temperature and salinity are promising data sources to investigate surface horizontal thermohaline compensation at mesoscale and are a complementary tool to Argo (*Johnson et al.*, 2012; *Sabia et al.*, 2013). Although the data provided by SMOS still suffer from bias and noise, they present the advantage of an unprecedented consistent monthly coverage of SSS data between 40° N–S with an accuracy of 0.15 within a 100x100 km² and one month resolution (*Hernandez et al.*, 2014). The microwave SST has proven for a long time to be a valid and efficient data source for oceanography and climate studies although its precision is less than the one of infrared products but its spatio–temporal coverage is much better as it is very little affected by clouds.

Acknowledgments : N. Kolodziejczyk was supported by a CNES (French National Space Agency) post–doctoral grant. This work is supported by the SMOS/TOSCA CNES project and the ESA

STSE SMOS+SOS project. The LOCEAN_v2013 Sea Surface Salinity maps have been produced by LOCEAN/IPSL (UMR CNRS/UPMC/IRD/MNH) laboratory that participates to the Ocean Salinity Expertise Center (CECOS) of Centre Aval de Traitement des Données SMOS (CATDS). The ISAS and Argo data are kindly provided by Fabienne Gaillard and freely available on request on <http://wwz.ifremer.fr/lpo/La-recherche/Projets-en-cours/GLOSCAL/Global-T-S-analysis> (LPO, CNRS/Ifremer/IRD/UBO, Brest, France) and funded by the CNES-TOSCA project 'GLOSCAL'. Sea Surface Salinity data derived from thermosalinograph instruments installed on board the 'MN *Toucan*' and 'MN *Colibri*' voluntary observing ships were collected, validated, archived, and made freely available by the French Sea Surface Salinity Observation Service (SO-SSS; <http://www.legos.obs-mip.fr/observation/sss/>). TMI data are produced by Remote Sensing Systems and sponsored by the NASA Earth Science MEASUREs DISCOVER Project. The surface velocity data derived from altimetry fields were produced by Ssalto/Duacs and distributed by Aviso with support from Cnes (<http://www.aviso.altimetry.fr/duacs/>). The authors acknowledge OceanColor and NASA for freely providing the Chlorophyll-a MODIS L3 products (<http://oceancolor.gsfc.nasa.gov>). The authors thanks Dr. Christopher W. Brown for many corrections and suggestions on the manuscript. The authors thanks anonymous reviewers that contribute to improve the manuscript.

References

- Alves J. L.G. R., and A. Colin de Verdière (1999), Instability Dynamics of a Subtropical Jet and Applications to the Azores Front Current System: Eddy-Driven Mean Flow, *J. Phys. Oceanogr.*, 29, 832–864.
- Bingham, F. M., G. R. Foltz, M. J. McPhaden (2012), Characteristics of the seasonal cycle of the surface layer salinity in the global ocean, *Ocean Sci.*, 915–929, doi: 10.5194/os-8-915-2012.
- Boutin, J., Waldteufel, P., Martin, N., Caudal, G., and Dinnat, E. (2004), Surface Salinity Retrieved from SMOS Measurements over the Global Ocean: Imprecisions Due to Sea Surface Roughness and Temperature Uncertainties, *J. Atm. Oceanic Tech.*, 21, 1432-1447, doi:10.1175/1520-0426(2004)021i1432:ssrfsm&2.0.co;2 .
- Boutin, J., N. Martin , G. Reverdin , X. Yin , and F. Gaillard (2013), Sea surface freshening inferred from SMOS and ARGO salinity: impact of rain, *Ocean Sci.*, 9, 183-192 , doi:10.5194/os-9-183-2013.
- Busecke, J., A. L. Gordon, Z. Li, F. M. Bingham, and J. Font (2014): Subtropical surface layer salinity budget and the role of mesoscale turbulence, *J. Geophys. Res.*, *accepted*, DOI 10.1002/2013JC009715.
- Chelton, D. B., R. A. de Szoeke, and M. G. Schlax (1998), Geographical variability of the first Rossby braoclinic radius of deformation, *J. Phys. Oceanogr.*, 28, 433–460.
- Cole, S. T., D. L. Rudnick, and J. A. Colosi (2010), Seasonal evolution of upper-ocean horizontal structure and the remnant mixed layer, *J. Geophys. Res.*, 115, C04012,

doi:10.1029/2009JC005654 .

- Cole, S. T., and D. L. Rudnick (2012), The spatial distribution and annual cycle of upper ocean thermohaline structure, *J. Geophys. Res.*, 117, C02027, doi:10.1029/2011JC007033.
- Dong, C., McWilliams J. C., Liu, Y., and D. Chen, (2014): Global heat and salt transports by eddy movement, *Nature Communications*, 5, 3294, doi:10.1038/ncomms4294.
- Ferrari, R., and D. L. Rudnick (2000), Thermohaline variability in the upper ocean, *J. Geophys. Res.*, 105, 16,857–16,883, doi:10.1029/2000JC900057.
- Ferrari, R., and F. Paparella (2003), Compensation and alignment of the thermohaline gradient in the ocean mixed layer, *J. Phys. Oceanogr.*, 33, 2214–2223.
- Fisher, N. I. (1993), Statistical Analysis of Circular Data, *Cambridge University Press*.
- Font, J., A. Camps, A. Borges, M. Martín-Neira, J. Boutin, N. Reul, Y. H. Kerr, A. Hahne, S. Mecklenburg, (2010): SMOS: the challenging sea surface salinity measurement from space. *Proceedings of the IEEE*, 98(5), 649–665 doi:10.1109/JPROC.2009.2033096.
- Gaillard, F., E. Autret, V. Thierry, P. Galaup, C. Coatanoan, and T. Loubrieu (2009), Quality Control of Large Argo Datasets, *J. Atmos. And Oceanic Tech.*, 26, 337–351.
- Gentemann, C. L., F. J. Wentz, C. A. Mears, and D. K. Smith (2004), In situ validation of Tropical Rainfall Measuring Mission microwave sea surface temperatures, *J. Geophys. Res.*, 109, C04021, doi:10.1029/2003JC002092.
- Gordon, A. L., and C. F. Giulivi (2012), Ocean eddy freshwater flux convergence into the North Atlantic subtropics, *J. Geophys. Res.*, 119, 3327–3335, doi:10.1002/2013JC009596.

- Grodsky, S. A., G. Reverdin, J. A. Carton, and V. J. Cole (2014a), Year-to-year salinity changes in the Amazon plume: Contrasting 2011 and 2012 Aquarius/SACD and SMOS satellite data, *Remote Sensing of Environment*, 140,14–22, doi: 10.1016/j.rse2013.08.033.
- Grodsky, S. A., J. A. Carton, and F. O. Bryan (2014b), A curious local surface salinity maximum in the northwestern tropical Atlantic, *J. Geophys. Res.*, 119, 484–495, doi:10.1002/2013JC009450.
- Hasson, A., T. Delcroix, and J. Boutin (2013), Formation and variability of the South Pacific Sea Surface Salinity maximum in recent decades, *J. Geophys. Res.*, 118(10), 5109–5116.
- Hernandez, O., J. Boutin, N. Kolodziejczyk, G. Reverdin, N. Martin, F. Gaillard, N. Reul, and J. L. Vergely (2014), SMOS salinity in the subtropical north Atlantic salinity maximum: Part I: Comparison with Aquarius and in situ salinity, *J. Geophys. Res.*, doi: 10.1002/2013JC009610 .
- Iselin, C. O. D. (1939), The influence of vertical and lateral turbulence on the characterization of waters at mid-depth, *EOS Trans. AGU*, 414–417.
- Johnson, G. C., S. Schimidtko, and J. M. Lyman (2012), Relative contributions of temperature and salinity to seasonal mixed layer density changes and horizontal density gradients, *J. Geophys. Res.*, 117, C04015, doi:10.1029/2011JC007651.
- Juliano, F. M., and M. L. G. R. Alves (2007), The Atlantic Subtropical Front/Current Systems of Azores and St. Helena , *J. Phys. Oceanogr.*, 37, 2573–2598 , doi: 10.1175/2007JPO3150.1

- Kainulainen, J., Colliander, A., Closa, J., Martin-Neira, M., Oliva, R., Buenadicha, G., Rubiales Alcaine, P., Hakkarainen, A., and Hallikainen, M. T. (2012), Radiometric Performance of the SMOS Reference Radiometers - Assessment After One Year of Operation, *IEEE Trans. Geosci. Remote Sens.*, 50, 1367-1383, doi:10.1109/tgrs.2011.2177273.
- Kolodziejczyk, N., and F. Gaillard (2012), Interannual variability of spiciness in the Pacific pycnocline, *J. Geophys. Res.*, 117, C12018, doi:10.1029/2012JC008365.
- Kolodziejczyk, N., and F. Gaillard (2013), Variability of the Heat and Salt Budget in the Subtropical South-Eastern Pacific Mixed Layer between 2004 and 2010: Spice Injection Mechanism, *J. Phys. Oceanogr.*, 43, 1880-1898.
- Marshall, J., and F. Schott (1999), Open-ocean convection: observations, theory and models, *Rev. Geophys.*, 37, 1, 1-64.
- Mignot, J., A. Lazar, and M. Lacarra (2012), On the formation of barrier layers and associated vertical temperature inversions: A focus on the northwestern tropical Atlantic, *J. Geophys. Res.*, 117, C02010, doi:10.1029/2011JC007435 .
- Oliva, R., E. Daganzo-Eusebio, Y. H. Kerr, S. Mecklenburg, S. Nieto, P. Rchaume, and C. Gruhier (2012), SMOS Radio Frequency Interference scenario: Status and actions taken to improve the RFI environment in the 1400-1427-MHz passive band, *IEEE Trans. Geos. Remote Sens.*, 30, 5, 1427-1439.
- Reul, N., B. Chapron, T. Lee, C. Donlon, J. Boutin and G. Alory, 2014: Sea Surface Salinity structure of the meandering Gulf Stream revealed by SMOS sensor, *Geophys. Res.*

Letts., accepted with minor modifications.

- Reul, N., S. Fournier, J. Boutin, O. Hernandez, B. Chapron, G. Alory, Y. Quilfen, J. Tenerelli, S. Morriset, Y. Kerr, S. Mecklenburg, and S. Delwart (2013), Sea Surface Salinity Observations from Space with the SMOS Satellite: A New Means to Monitor the Marine Branch of the Water Cycle, *Surveys of Geophys*, 1-42, doi:10.007/s10712-013-9244-0.
- Reul, N., J. Tenerelli, J. Boutin, B. Chapron, F. Paul, E. Brion, F. Gaillard, and O. Archer, 2012: Overview of the First SMOS Sea Surface Salinity Products. Part I: Quality Assessment for the Second Half of 2010, *IEEE transactions on geographical and remote sensing*, Vol. 50, No. 5, pp. 1636-1647, DOI: 10.1109/TGRS.2012.2188408.
- Reverdin, G., E. Kestenare, C. Franckignoul, and T. Delcroix (2007), Surface salinity in the Atlantic Ocean (30° S-50° N) , *Prog. Oceanogr.*, 73, 311-340.
- Roden, G., I (1974), Thermohaline structure, fronts and sea-air energy exchange of the trade wind region east of Hawaii, *J. Phys. Oceanogr.*, 4, 168-182, doi:10.1175/1520-0485(1974)004<0168:TSFASA>2.0.CO;2.
- Roden, G. I. (1991), Mesoscale flow and thermocline structure around Fieberling Seamount, *J. Geophys. Res.*, 96, 16,653-16,672, doi: 10.1029/91JC01747.
- Ruddick, B., (1983), A practical indicator of stability of the water column to double-diffusive activity, *Deep-Sea Res.*, 30A, 1,105-1,107.
- Rudnick, D. L., and J. R. Luyten (1996), Intensive surveys of the Azores Front. 1. Tracers and dynamics, *J. Geophys. Res.*, 101, C1, 923-939.

- Rudnick, D. L., and R. Ferrari (1999), Compensation of the horizontal temperature and salinity gradient in the ocean mixed layer, *Science*, 283, 526–529.
- Rudnick, D. L., and J. P. Martin (2002), On the horizontal density ratio in the upper ocean, *Dyn. Atm. Ocean*, 36, 3–21.
- Tanguy Y., S. Arnault, and P. Lattes (2010): Isothermal, mixed layers and barriers layers in the tropical and sub-tropical Atlantic ocean during the ARAMIS experiment. *Deep Sea Res. I*, doi:10.1016/j.dsr.2009.12.012.
- Sabia, R., M. Klockmann, C. Donlon *et al.* (2013), Satellite-Based T-S Diagrams: A Prospective Tool to Trace Ocean Water Masses, *Proceedings of ESA Living planet symposium*, 9–13 Sep. 2013, Edinburg, UK,
- Stommel, H. M. (1979), Determination of water mass properties of water pumped down from Ekman layer to the geostrophic flow below, *Proc. Natl. Acad. Sci. U.S.A.*, 76, 3051–3055, doi:10.1073/pnas.76.7.3051.
- Stommel, H. M. (1993), A conjectural regulating mechanism for determining the thermohaline structure in the ocean mixed layer, *J. Phys. Oceanogr.*, 23, 142–148.
- Volkov, D. L., and L.-L. Fu (2010), On the Reasons for the Formation and Variability of the Azores Current, *J. Phys. Oceanogr.*, 40, 2197–2220.
- Yeager, G. S., and W. G. Large (2007), Observational Evidence of Winter Spice Injection, *J. Phys. Oceanogr.*, **37**, 2895–2019.
- Young, W. R. (1994), The subinertial mixed layer approximation, *J. Phys. Oceanogr.*, 24, 1812–1826.

Figures captions:

Figure 1: August 2011 SSS map from monthly SMOS smoothed data at $100 \times 100 \text{ km}^2$ in the Subtropical–tropical Atlantic. 14 TSG transects (black tracks) across the SSS maximum from June 2010 and October 2011 and one between August 7–15 2011 (green track). The $28\text{--}40^\circ \text{ N}/45\text{--}25^\circ \text{ W}$ box is depicted in a thick black line and the thick black contour within the box shows the 36.6 isohaline chosen to illustrate the Azores Front/Current. The isohaline contours are shown in thin black line contour. C.I. = 1.

Figure 2: Comparison of SMOS/TMI (thick red), ISAS (black) and TSG (blue) 500 km Butterworth–lowpass filtered salinity (a); temperature in $^\circ \text{C}$ (b) and density in $\text{kg}\cdot\text{m}^{-3}$ (c) collocated along TSG tracks between $10\text{--}40^\circ \text{ N}$ over 7–15 August 2011 (see Table 1). Contribution of the horizontal temperature (a) and salinity (b) gradients to the resulting horizontal density gradient ($\text{kg}\cdot\text{m}^{-4}$).

Figure 3: Probability Density Function (PDF; in color) of 500 km Butterworth–lowpass filtered (a) TSG SSS gradient vs collocated ISAS SSS gradient; (b) TSG SSS gradient vs collocated SMOS SSS gradient; (c) TSG SST gradient vs collocated ISAS SST gradient; (d) TSG SST gradient vs collocated TMI SST gradient. The calculation has been done for the 14 TSG transects available between July 2010 and December 2011

listed in the Table 1.

Figure 4: March and August mean surface salinity (ab and gh); temperature in $^{\circ}$ C (cd and ij); density in kg.m^{-3} (ef and kl) computed from ISAS (left column) and SMOS/TMI (right column) products smoothed over $3 \times 3^{\circ}$ between July 2010 and December 2012. The black contours represent the mean March (a-f) and August (g-l) salinity. Note that, the white squares of missing data in filtered fields correspond to island contaminations.

Figure 5: March and August median norm of the near surface density gradient in kg.m^{-4} (ab and gh); density ratio $\text{atan}/R/$ in degrees with the corresponding $|R|$ scale (cd and ij); mean angle M_{ϕ} of thermohaline gradient in degrees (ef and kl) between July 2010 and December 2012. The black contours represent the salinity seasonal standard deviation. Note that, the white squares of missing data in filtered fields correspond to island contaminations.

Figure 6: Comparison of SMOS/TMI (thick red), ISAS (black) and TSG (blue) 200–500 km Butterworth–bandpass filtered salinity (a); temperature in $^{\circ}$ C (b) and density in kg.m^{-3} (c) collocated along TSG tracks between $10\text{--}40^{\circ}$ N over 7–15 August 2011 (see Table 1). Contribution of the horizontal temperature (a) and salinity (b)

gradients to the resulting horizontal density gradient (kg.m^{-4}).

Figure 7: Probability Density Function (PDF; in color) of 200–500 km Butterworth–bandpass filtered (a) TSG SSS gradient vs collocated ISAS SSS gradient; (b) TSG SSS gradient vs collocated SMOS SSS gradient; (c) TSG SST gradient vs collocated ISAS SST gradient; (d) TSG SST gradient vs collocated TMI SST gradient. The calculation was done for the 14 TSG transects available between July 2010 and December 2011 listed in the Table 1.

Figure 8: March 2012 monthly mean surface salinity from (a) SMOS and (b) ISAS, surface temperature in $^{\circ}\text{C}$ from (c) TMI (d) ISAS, and surface density in kg.m^{-3} from (e) SMOS/TMI and (f) ISAS. Arrows are monthly mean geostrophic surface velocities (in m.s^{-1}) from AVISO. The thick black contour corresponding to the $8 \cdot 10^{-5} \text{ s}^{-5}$ vorticity isoline identifies the Azores Front/Current ($vort = f + \xi$; where f is the planetary vorticity and ξ is the relative vorticity computed as $\xi = \partial v / \partial x - \partial u / \partial y$). The thick magenta (blue) contours corresponding to the 36.6 isohaline (19°C isotherm) identify the thermohaline front associated with the Azores front. Colored circle are at the Argo float position and the corresponding near-surface (~ 5 m depth) salinity, temperature and salinity values.

Figure 9: March 2012 monthly SMOS/TMI (a) density gradient surface salinity in kg.m^{-4} , (b) norm of the density ratio $\text{atan}|R|$ in $^\circ$, (c) $\text{angle}(R)$ between temperature and salinity gradient vector in $^\circ$. Arrows indicate the monthly mean geostrophic surface velocities from AVISO (in m.s^{-1}). Thick black, magenta and blue contours are the same as in Fig. 7.

Figure 10: July 2011 monthly mean surface salinity from (a) SMOS and (b) ISAS, surface temperature in $^\circ \text{C}$ from (c) TMI and (d) ISAS, (e) MODIS sea surface Chlorophyll-a concentration in $\log(\text{kg.m}^{-3})$, and surface density in kg.m^{-3} from (f) SMOS/TMI and (g) ISAS. Arrows are the monthly mean geostrophic surface velocities from AVISO (in m.s^{-1}). Thick black and magenta contours and colored circles are the same as in Fig. 7.

Figure 11: Same as Figure 9, except for July 2011.

Figure 12: SMOS SSS 10-day mean (ab); TMI SST weekly mean (cd) in $^\circ \text{C}$, and density computed from SMOS and TMI (ef) in kg.m^{-3} taken from satellite measurements between 11-21 March 2011 and 10-17 March 2011, respectively. The black square delimits the region $25-39^\circ \text{N}$ and $40-30^\circ \text{W}$ (bdf). The colored circles represent the individual Argo temperature and salinity near surface measurements taken at about 5

m depth between March 11–21 2011. Gray arrows present the geostrophic surface velocities deduced from AVISO in $\text{m}\cdot\text{s}^{-1}$ averaged between March 11–21 2011.

Tables

Table 1: List of merchant ships TSG transects: ship name in second column; third and fourth columns indicate the start date and the end date of the transect between 40–10° N; and the last column gives the percentage of missing salinity measurements.

| | Ship | Start date | End date | % S missing val. |
|----|---------|-------------|-------------|------------------|
| 1 | Toucan | 20 Jun 2010 | 29 Jun 2010 | 2.0 |
| 2 | Colibri | 30 Jun 2010 | 8 Jul 2010 | 0.0 |
| 3 | Toucan | 10 Jul 2010 | 20 Jul 2010 | 5.2 |
| 4 | Colibri | 13 Aug 2010 | 23 Aug 2010 | 0.8 |
| 5 | Colibri | 17 Oct 2010 | 30 Oct 2010 | 2.3 |
| 6 | Colibri | 19 Dec 2010 | 2 Jan 2011 | 0 |
| 7 | Colibri | 5 Jan 2011 | 20 Jan 2011 | 1.2 |
| 8 | Toucan | 29 Jan 2011 | 7 Feb 2011 | 0.4 |
| 9 | Toucan | 16 Feb 2011 | 23 Feb 2011 | 0.2 |
| 10 | Colibri | 28 Feb 2011 | 8 Mar 2011 | 0.1 |
| 11 | Colibri | 9 Jun 2011 | 17 Jun 2011 | 18.8 |
| 12 | Colibri | 7 Aug 2011 | 15 Aug 2011 | 0 |
| 13 | Colibri | 10 Oct 2011 | 30 Oct 2011 | 12.1 |
| 14 | Colibri | 30 Oct 2011 | 12 Nov 2011 | 7.6 |

Table 2: Summary of the different configurations of the potential temperature and salinity horizontal fluctuations corresponding to respective value of the norm $|R|$ (dimensionless) and phase Φ (in degrees) of the density ratio R .

| | $\Phi \rightarrow \pm 180^\circ$ | $\Phi \rightarrow 0^\circ$ |
|----------------------------------------|--------------------------------------------------------------------------------------------|---------------------------------------------------------------------------------------|
| $ R =1$ $\text{atan}(R)=45^\circ$ | dT and dS of opposite signs / comparable and additional contribution of T and S to density | dT and dS have the same signs/ T and S variations compensate: no variation in density |
| $ R <1$ $\text{atan}(R)<45^\circ$ | Opposite signs (constructive)/ Salinity dominates | Same sign (compensated)/ Salinity dominates |
| $ R >1$ $\text{atan}(R)>45^\circ$ | Opposite sign (constructive)/ Temperature dominates | Same sign (compensated)/ Temperature dominates |

Table 3:

Correlation coefficient (significant at 99%) for 500 km lowpass filtered gradients computed from temperature and salinity from TSG, ISAS, TMI and SMOS.

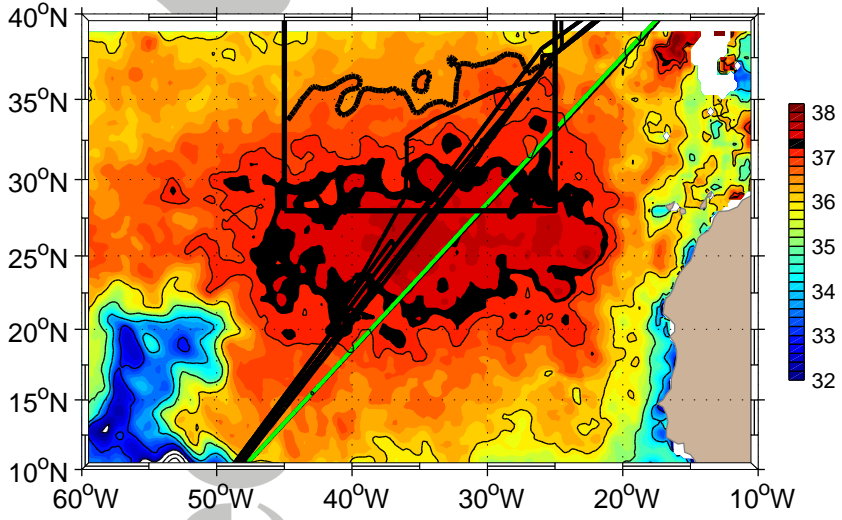
| | Date Transect | β dS/dl TSG/ISAS | β dS/dl TSG/SMOS | α dT/dl TSG/ISAS | α dT/dl TSG/TMI |
|----|---------------|---------------------------|---------------------------|----------------------------|---------------------------|
| 1 | 24-Jun-2010 | .99 | .92 | .45 | .85 |
| 2 | 15-Jul-2010 | .94 | .94 | .37 | .86 |
| 3 | 03-Aug-2010 | .91 | .95 | .55 | .67 |
| 4 | 18-Aug-2010 | .83 | .90 | .60 | .68 |
| 5 | 23-Oct-2010 | .68 | .84 | .90 | .62 |
| 6 | 26-Dec-2010 | .94 | .80 | .89 | .93 |
| 7 | 12-Jan-2011 | .94 | .92 | .83 | .98 |
| 8 | 02-Feb-2011 | .91 | .80 | .89 | .97 |
| 9 | 19-Feb-2011 | .88 | .94 | .89 | .93 |
| 10 | 04-Mar-2011 | .96 | .92 | .89 | .90 |
| 11 | 11-Jun-2011 | .81 | .91 | .74 | .85 |
| 12 | 11-Aug-2011 | .95 | .96 | .92 | .67 |
| 13 | 17-Oct-2011 | .89 | .97 | .62 | .89 |
| 14 | 20-Oct-2011 | .91 | .98 | .60 | .88 |
| | Mean | .90 | .91 | .70 | .83 |
| | STD | .08 | .05 | .19 | .12 |

Table 4: correlation of bandpass (200–500 km) filtered gradients between TSG, ISAS and SMOS
(significant at 99%).

| | Date Transect | β dS/dl TSG/ISAS | β dS/dl TSG/SMOS | α dT/dl TSG/ISAS | α dT/dl TSG/TMI |
|----|---------------|---------------------------|---------------------------|----------------------------|---------------------------|
| 1 | 24-Jun-2010 | .26 | .49 | -.10 | -.19 |
| 2 | 15-Jul-2010 | .31 | .28 | -.04 | .36 |
| 3 | 03-Aug-2010 | .44 | .79 | .78 | .04 |
| 4 | 18-Aug-2010 | -.02 | .77 | .62 | .78 |
| 5 | 23-Oct-2010 | -.11 | .75 | -.13 | .83 |
| 6 | 26-Dec-2010 | .40 | .17 | .32 | .64 |
| 7 | 12-Jan-2011 | .00 | .53 | .60 | .84 |
| 8 | 02-Feb-2011 | .63 | .62 | .46 | .73 |
| 9 | 19-Feb-2011 | .02 | .34 | -.19 | .96 |
| 10 | 04-Mar-2011 | -.33 | .36 | .04 | .63 |
| 11 | 11-Jun-2011 | .19 | .78 | -.07 | .30 |
| 12 | 11-Aug-2011 | .45 | .26 | -.10 | .65 |
| 13 | 17-Oct-2011 | -.06 | .03 | .17 | .42 |
| 14 | 20-Oct-2011 | .58 | .44 | .17 | .42 |
| | Mean | .20 | .47 | .18 | .53 |
| | STD | .29 | .24 | .32 | .33 |

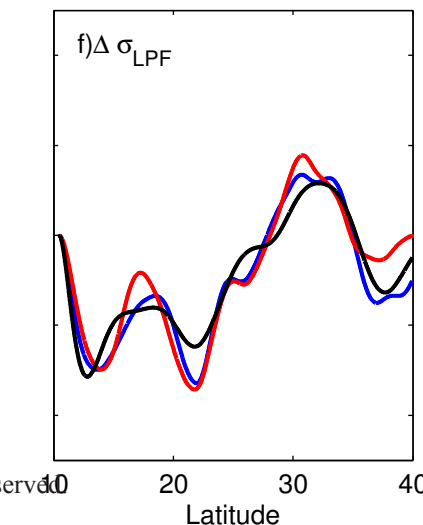
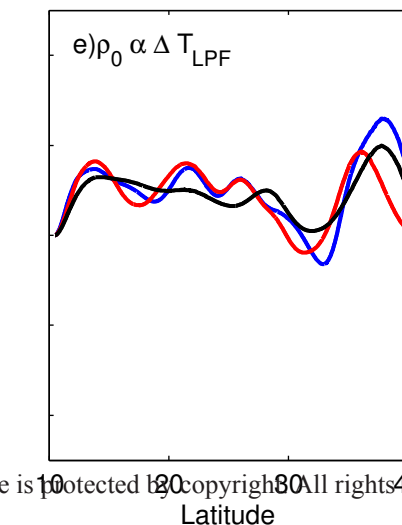
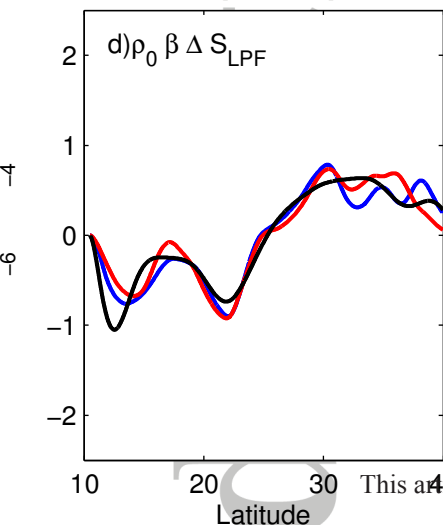
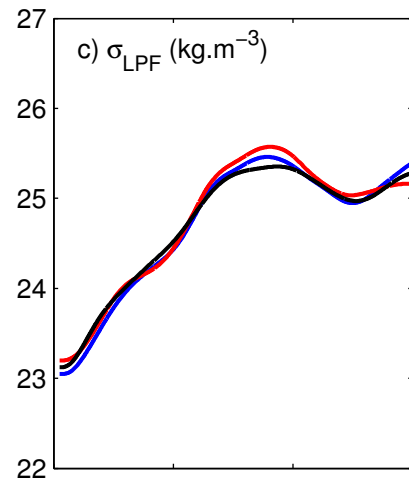
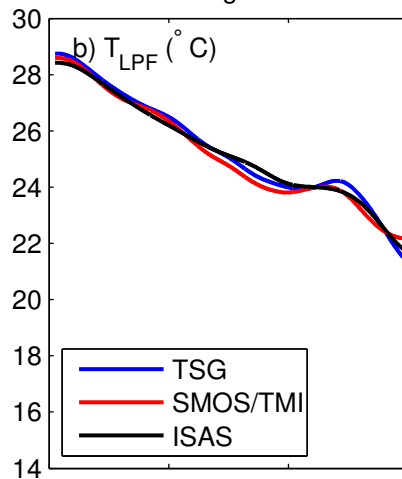
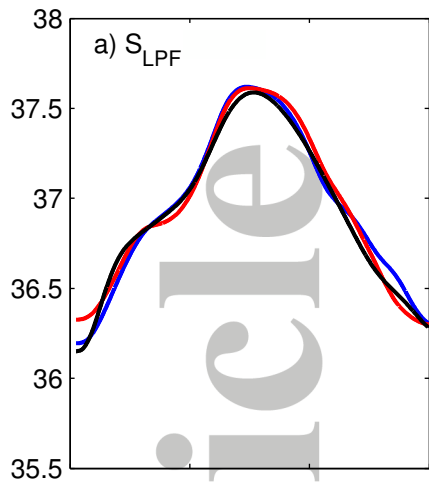
Article

August 2011

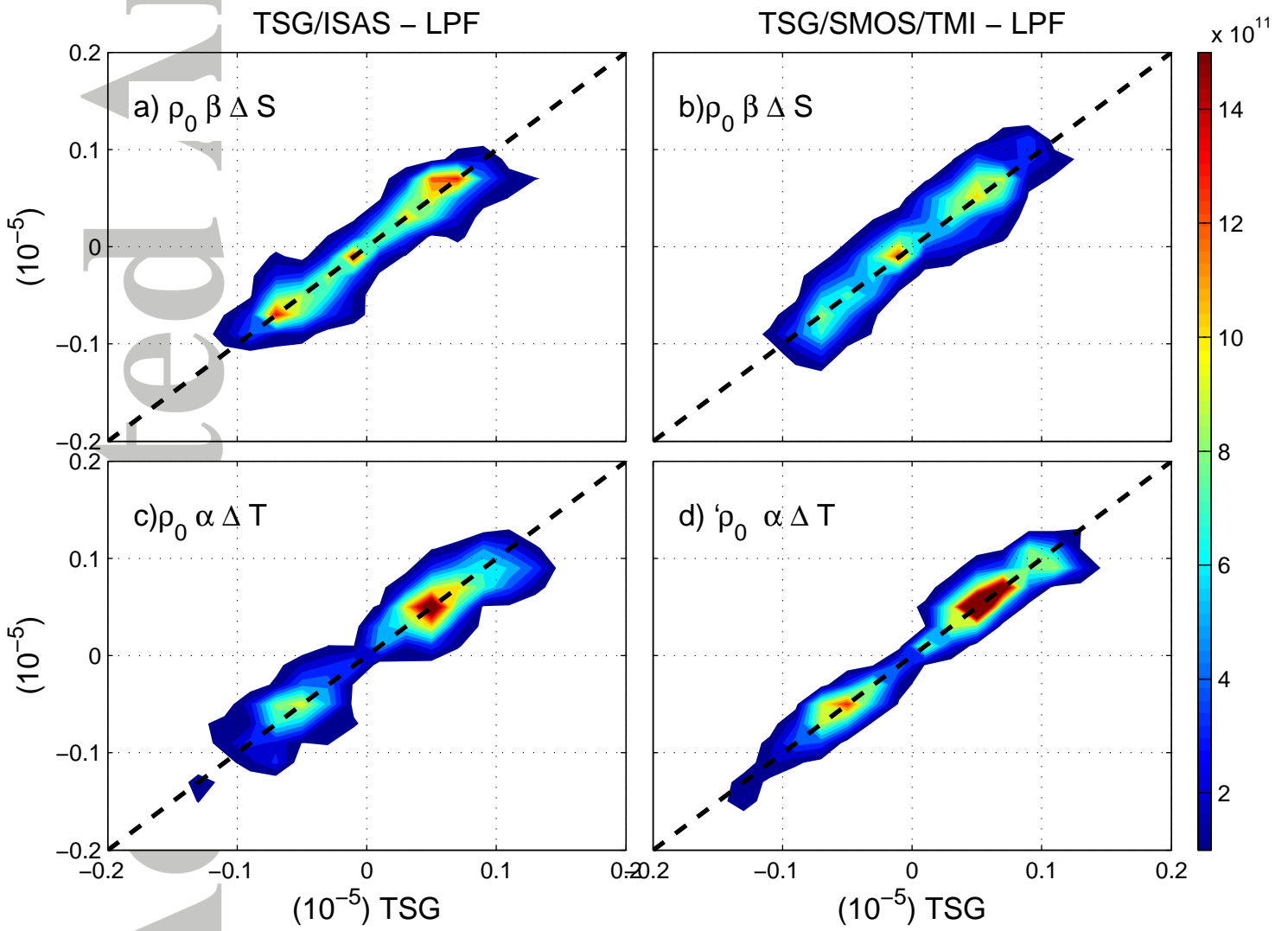


Accepted

11-Aug-2011



This article is protected by copyright. All rights reserved.



March

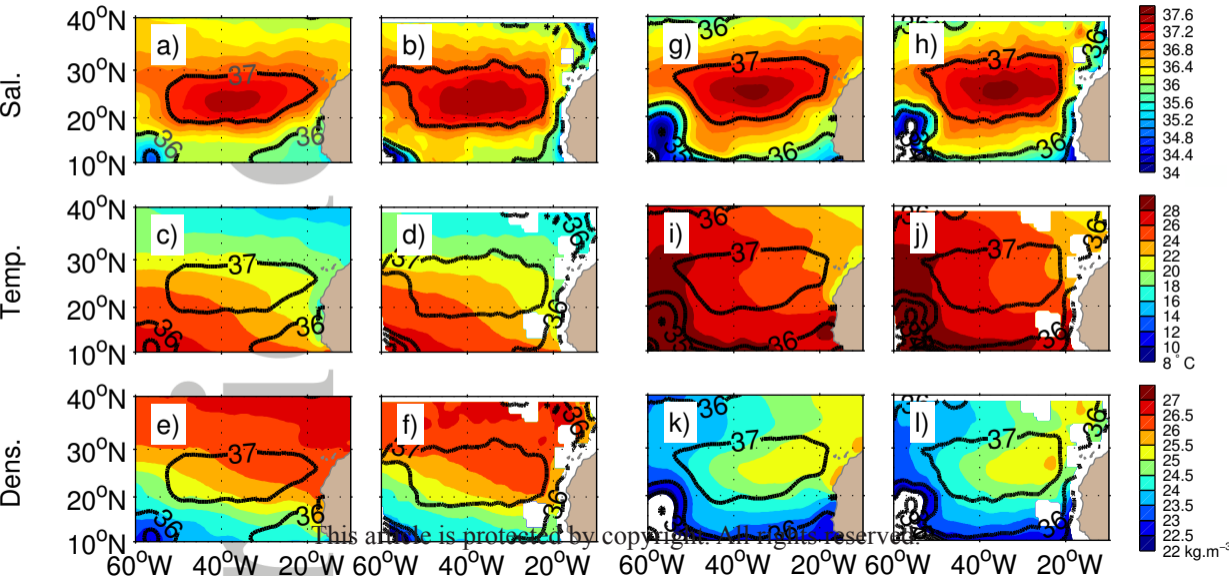
August

ISAS

SMOS/TMI

ISAS

SMOS/TMI



March

August

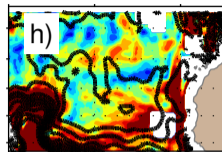
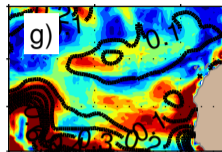
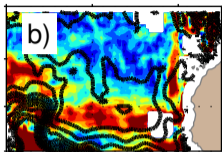
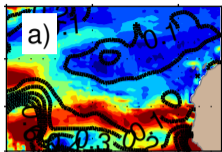
ISAS

SMOS/TMI

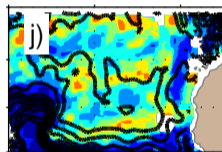
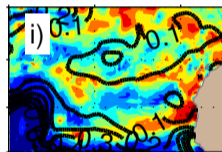
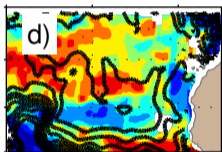
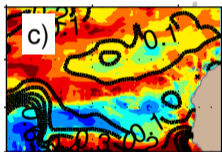
ISAS

SMOS/TMI

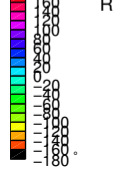
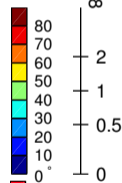
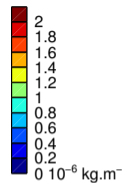
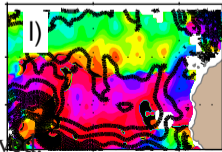
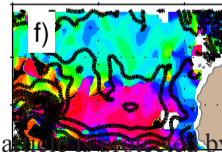
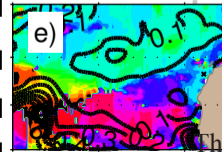
40°N
30°N
20°N
10°N



40°N
30°N
20°N
10°N



40°N
30°N
20°N
10°N

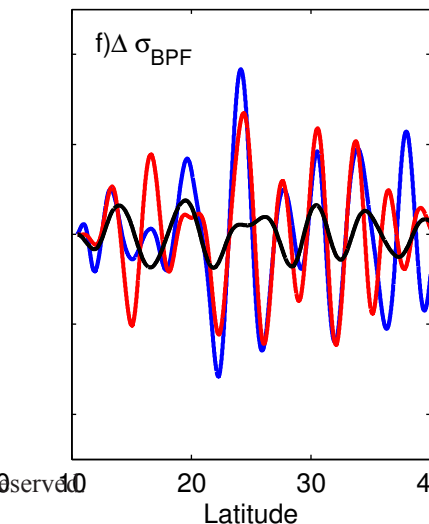
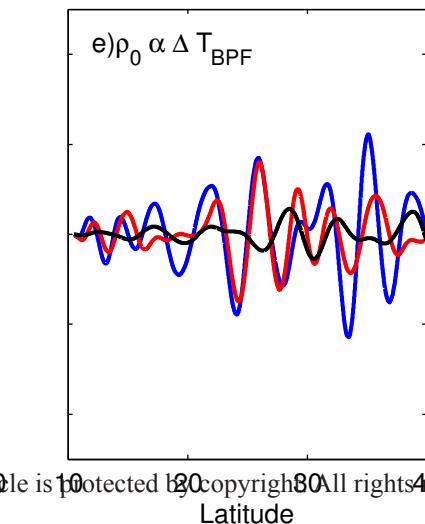
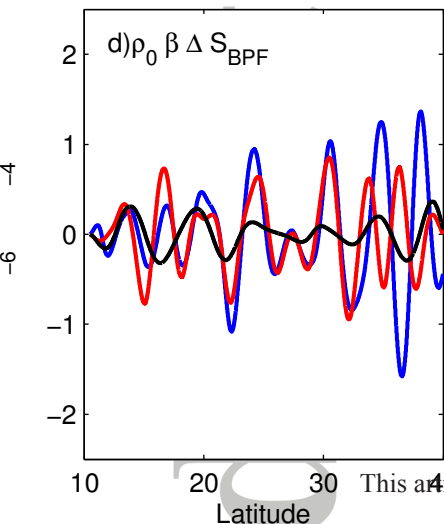
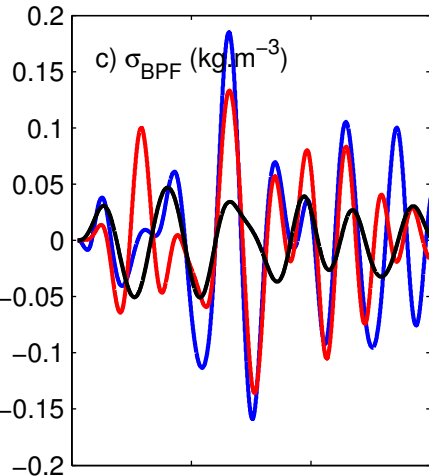
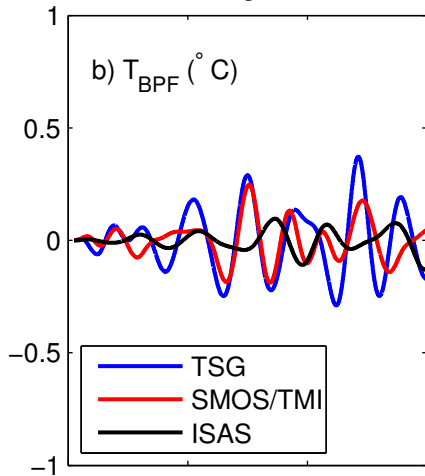
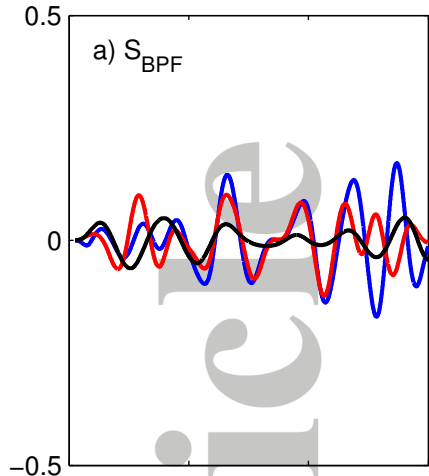


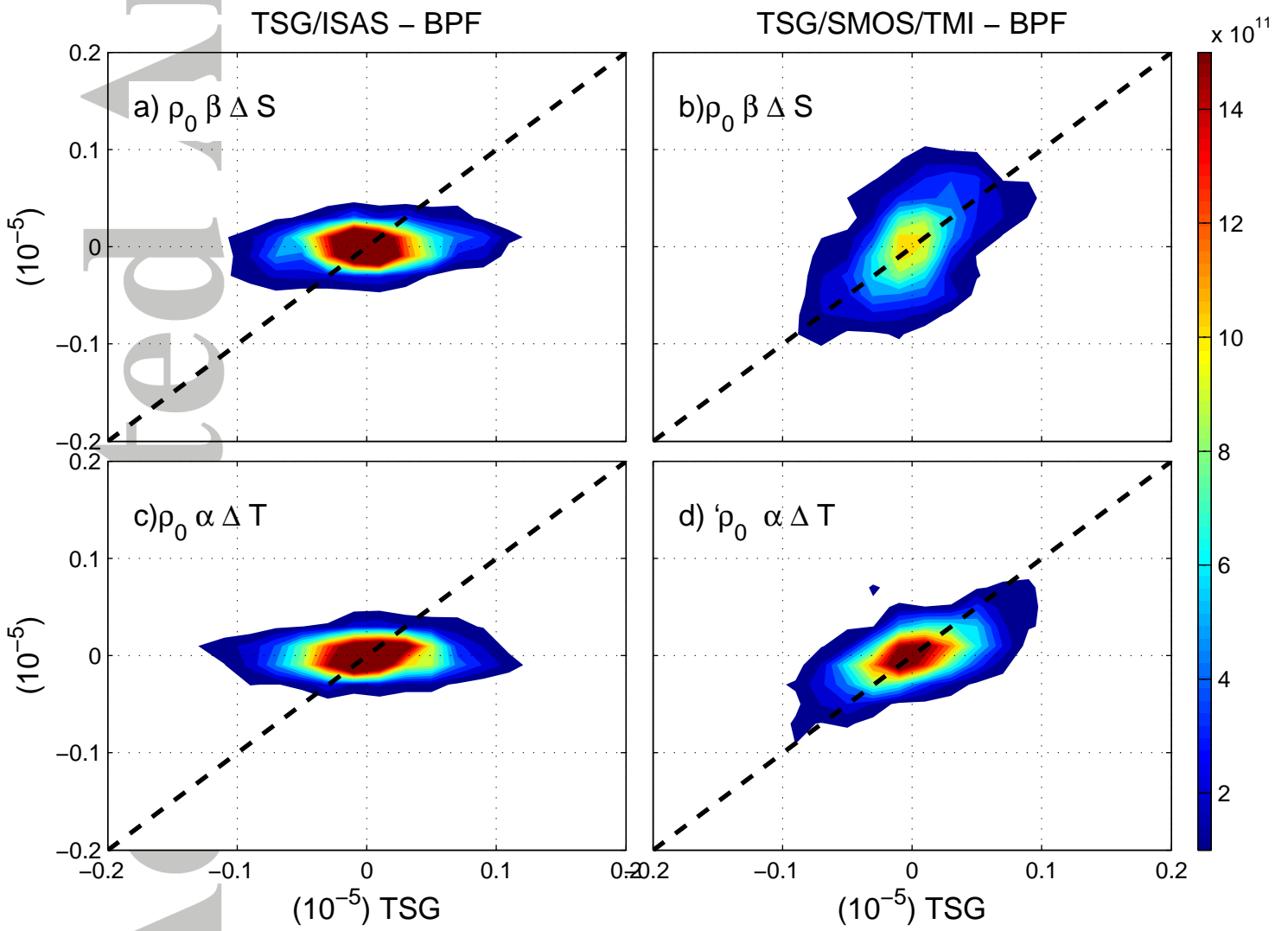
60°W 40°W 20°W 60°W 40°W 20°W 60°W 40°W 20°W 60°W 40°W 20°W

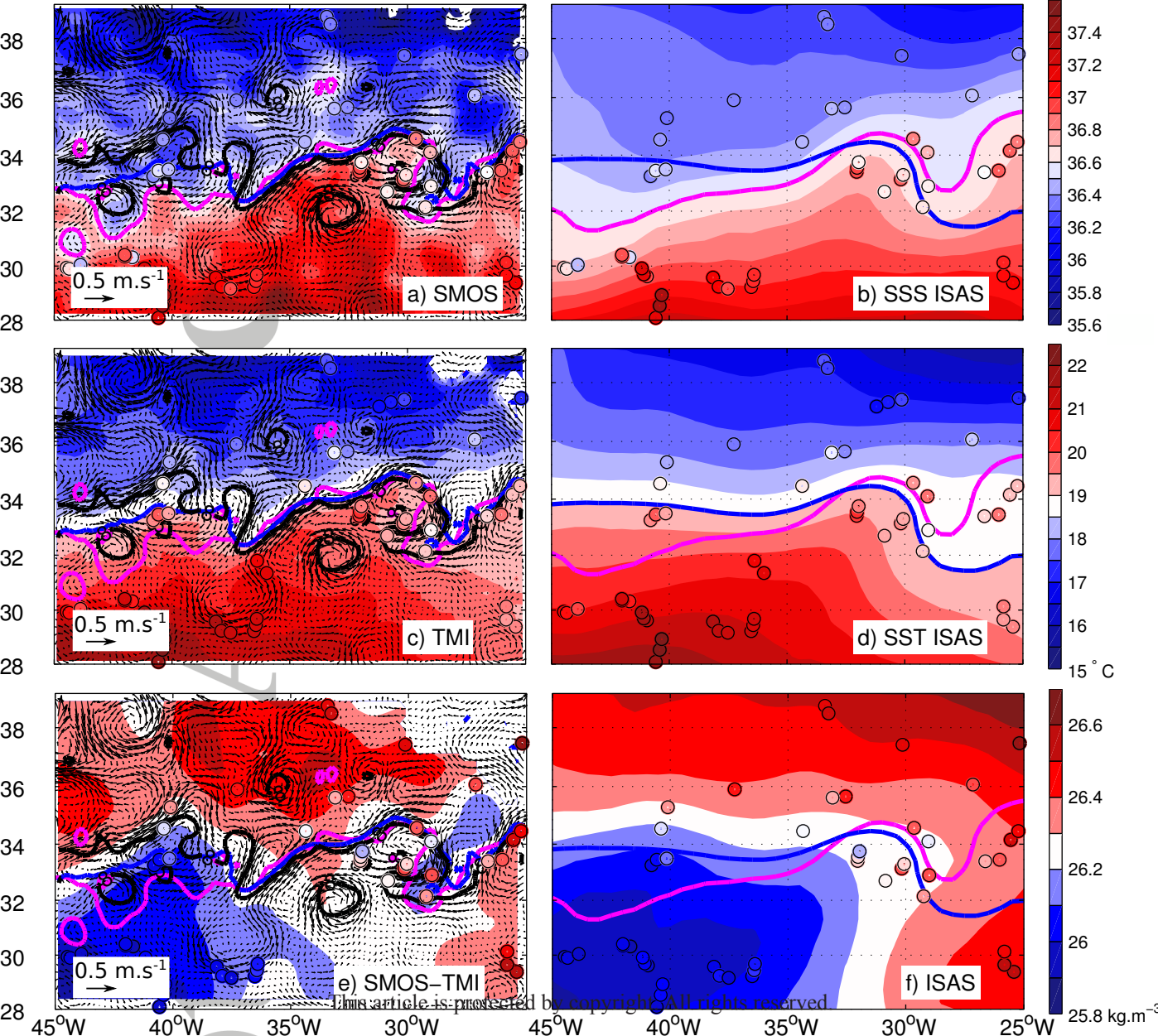
M

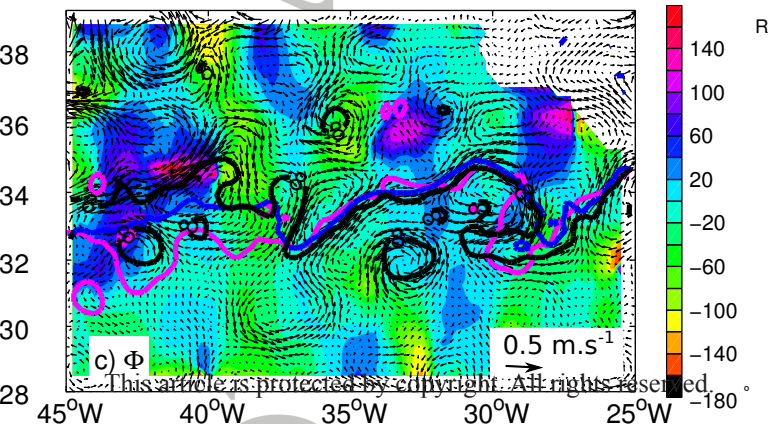
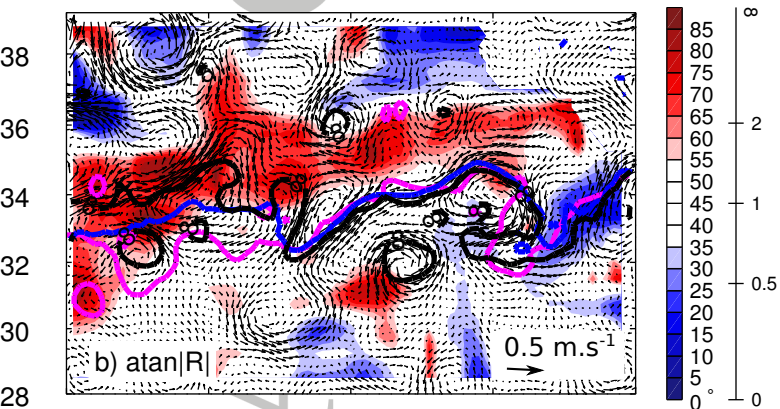
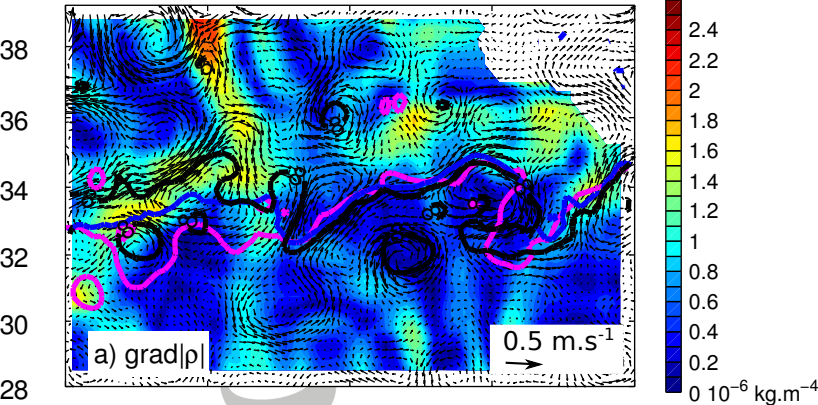
This article is copyrighted by copyright © 2013. All rights reserved.

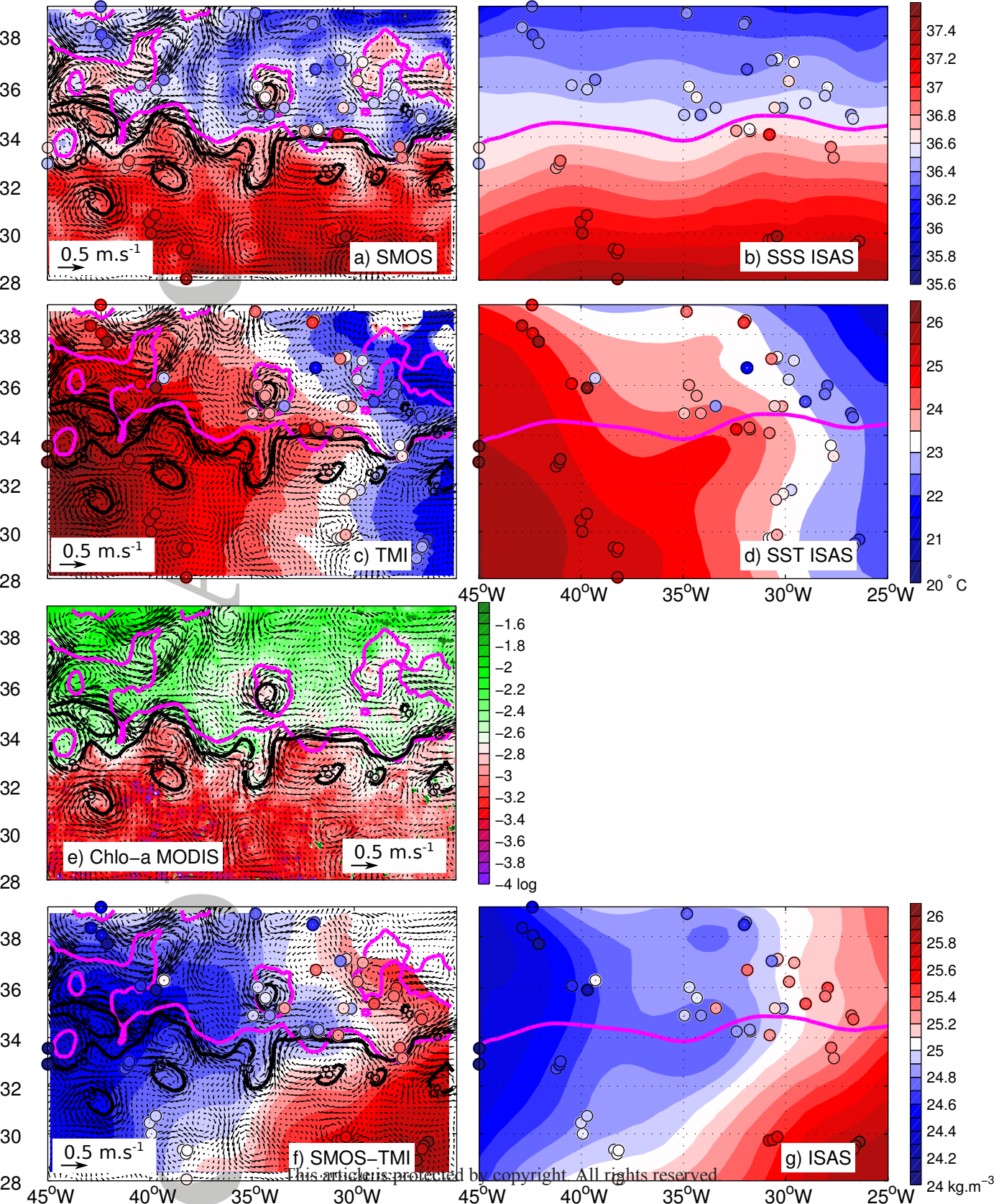
11-Aug-2011

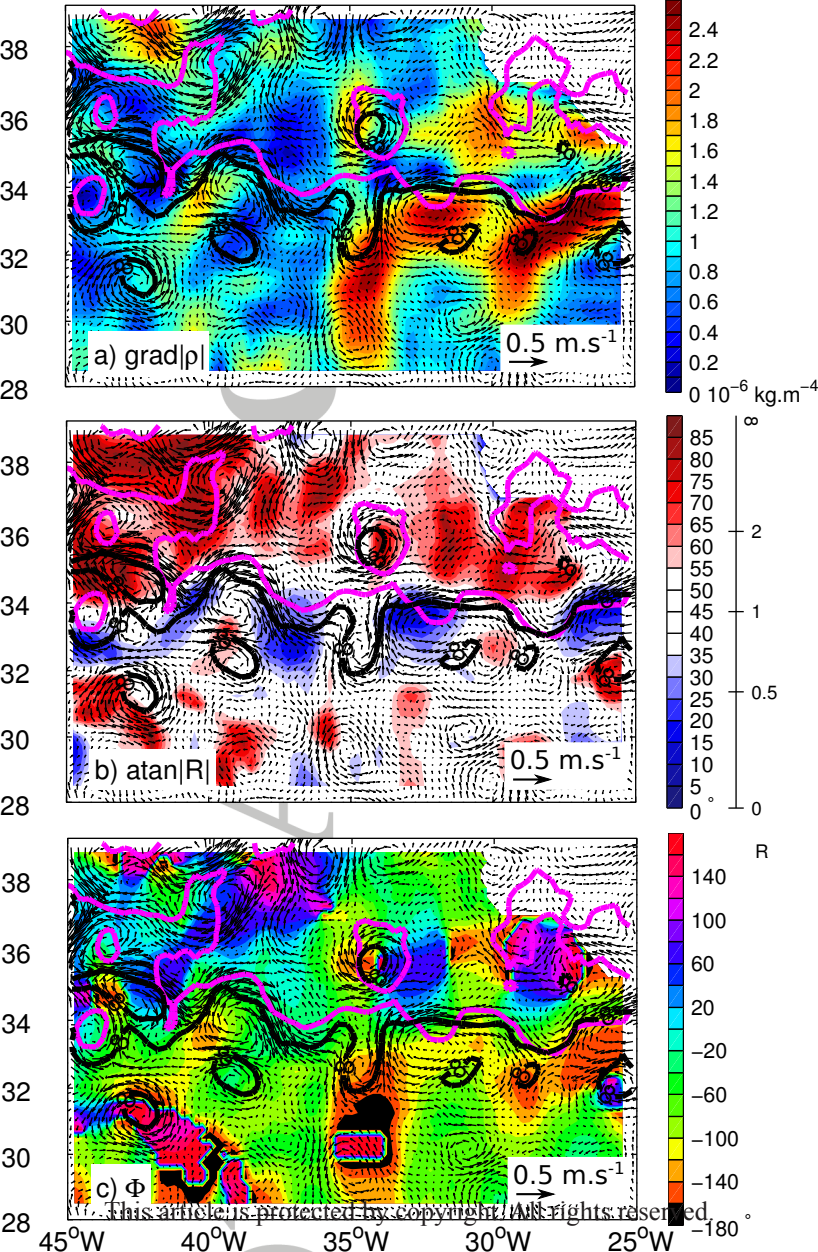




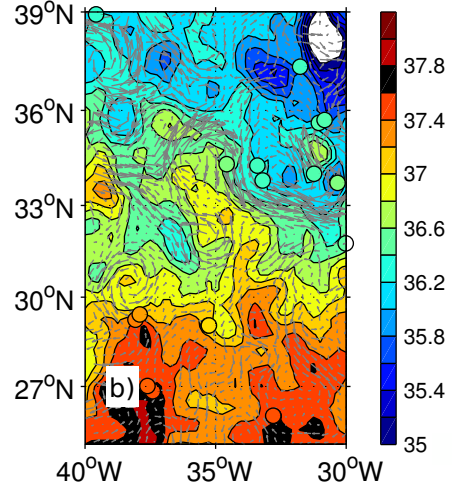
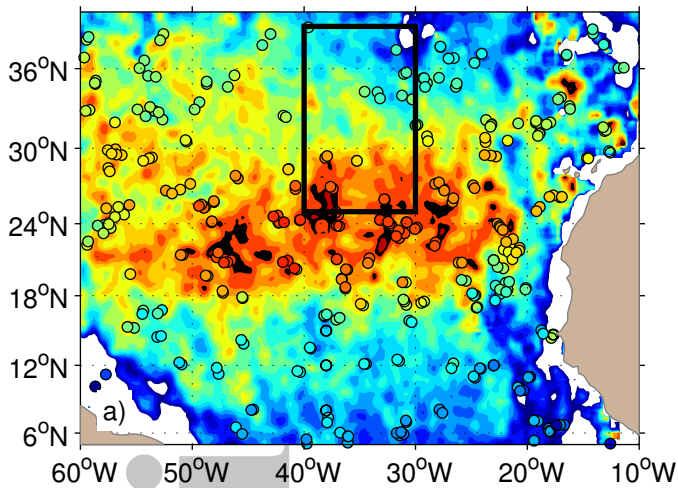




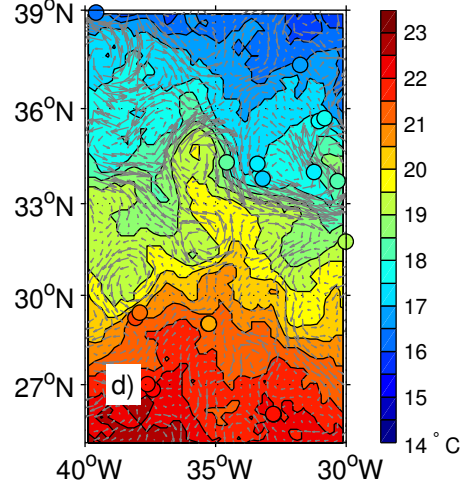
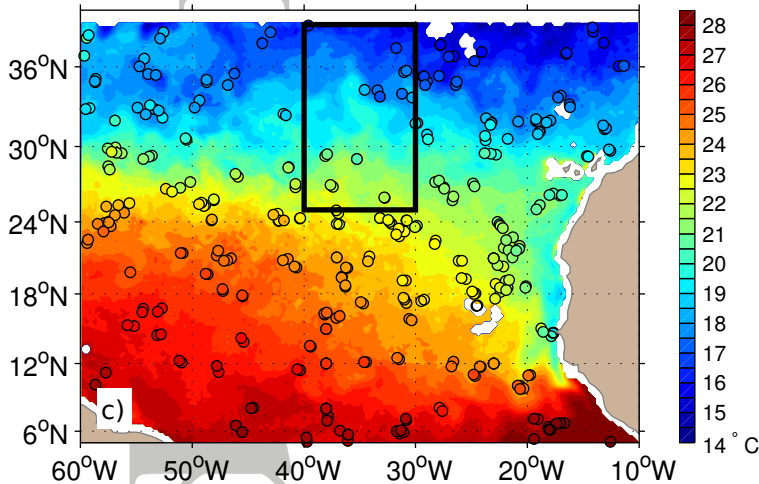




SMOS 10days16-Mar-2011



TMI Weekly12-Mar-2011



TMI/SMOS Density12-Mar-2011

